

# Supplementary Information - Interlayer Exciton in MoSe<sub>2</sub>/2D Perovskite Hybrid Heterostructures - Interplay Between Charge and Energy Transfer

M. Karpińska,<sup>†,‡,††</sup> J. Jasiński,<sup>¶,††</sup> R. Kempt,<sup>§</sup> J. D. Ziegler,<sup>||</sup> H. Sansom,<sup>⊥</sup> T. Taniguchi,<sup>#</sup> K. Watanabe,<sup>@</sup> H. J. Snaith,<sup>⊥</sup> A. Surrente,<sup>¶</sup> M. Dyksik,<sup>†,¶</sup> D. K. Maude,<sup>†</sup> Ł. Kłopotowski,<sup>‡</sup> A. Chernikov,<sup>||,△</sup> A. Kuc,<sup>\*,∇</sup> M. Baranowski,<sup>\*,¶</sup> and P. Plochocka<sup>\*,†,¶</sup>

<sup>†</sup>Laboratoire National des Champs Magnétiques Intenses, UPR 3228, CNRS-UGA-UPS-INSA, Grenoble and Toulouse, France

<sup>‡</sup>Institute of Physics, Polish Academy of Sciences, 02-668 Warsaw, Poland

<sup>¶</sup>Department of Experimental Physics, Faculty of Fundamental Problems of Technology, Wrocław University of Science and Technology, 50-370 Wrocław, Poland

<sup>§</sup>Technische Universität Dresden, Bergstr. 66c, 01062 Dresden, Germany

<sup>||</sup>Department of Physics, University of Regensburg, Regensburg D-93053, Germany

<sup>⊥</sup>University of Oxford, Clarendon Laboratory, Parks Road, Oxford, OX1 3PU, United Kingdom

<sup>#</sup>International Center for Materials Nanoarchitectonics, National Institute for Materials Science, Tsukuba, Ibaraki 305-004, Japan

<sup>@</sup>Research Center for Functional Materials, National Institute for Materials Science, Tsukuba, Ibaraki 305-004, Japan

<sup>△</sup>Dresden Integrated Center for Applied Physics and Photonic Materials (IAPP) and Würzburg-Dresden Cluster of Excellence ct.qmat, Technische Universität Dresden, 01062 Dresden, Germany

<sup>∇</sup>Helmholtz-Zentrum Dresden-Rossendorf, Permoserstraße 15, 04318 Leipzig, Germany

<sup>††</sup>Contributed equally to this work

E-mail: [a.kuc@hzdr.de](mailto:a.kuc@hzdr.de); [michal.baranowski@pwr.edu.pl](mailto:michal.baranowski@pwr.edu.pl); [paulina.plochocka@lncmi.cnrs.fr](mailto:paulina.plochocka@lncmi.cnrs.fr)

Figure S1 shows result of PL power depended measurements. No nonlinear effects are observed in the power range used.

Figure S2 shows broad range PL spectra of bare 2D perovskite layers. For BAPI emission related to defect (halide vacancies) can be observed. At a higher excitation power, a similar peak can be also observed in PEPI bare layer (see Fig. S1(a)). However, we did not observe any peak at the energies corresponding to the IX transition seen in the heterostructures. Additionally also when bare 2DPs are excited below the optical band gap, we do not observe

any emission in IX transition spectral range as shown in Fig. S3.

Figure S4 presents the first derivative of reflectivity spectrum of bare MoSe<sub>2</sub> (red curve) and in the heterostructure part (black curve) of PEPI/MoSe<sub>2</sub> - (a) and BAPI/MoSe<sub>2</sub> - (b). In both cases, monolayer MoSe<sub>2</sub> shows clear excitonic features related to X<sub>A</sub> and X<sub>B</sub> excitons. In the heterostructure region, we can observe an additional resonance, related to the absorption of the charged exciton T. Figure S5 shows the Brillouin zone and calculated band dispersion close to the band edges.

Figures S6 and S8 shows streak images of exciton and trion PL.

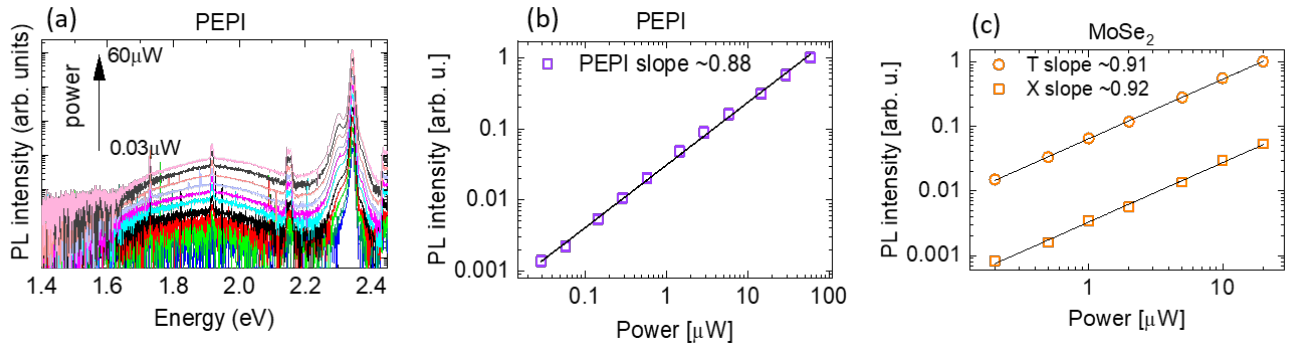


Figure S1: (a) PL spectra power dependence of bare PEPI layer in a log scale. (b) integrated PL intensity of PEPI exciton emission. (c) integrated PL intensity of  $\text{MoSe}_2$  exciton and trion emission.

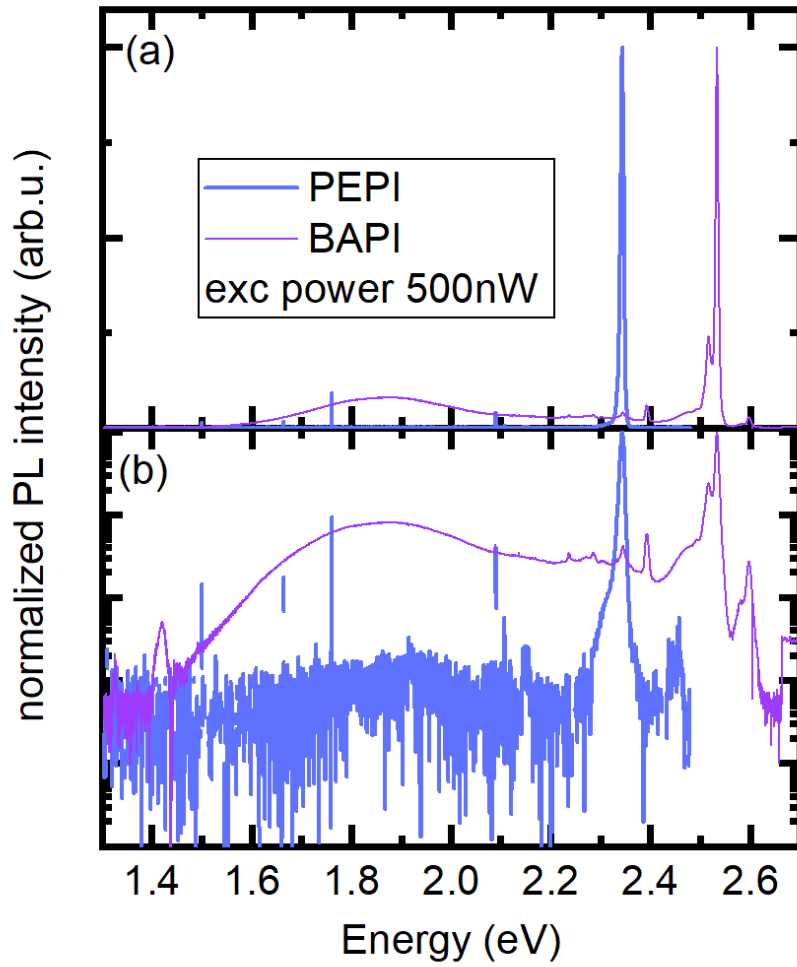


Figure S2: broad range PL spectra of bare PEPI and BAPI layer in a linear (a) and logarithmic (b) scale. No emission in IX energy range is observed.

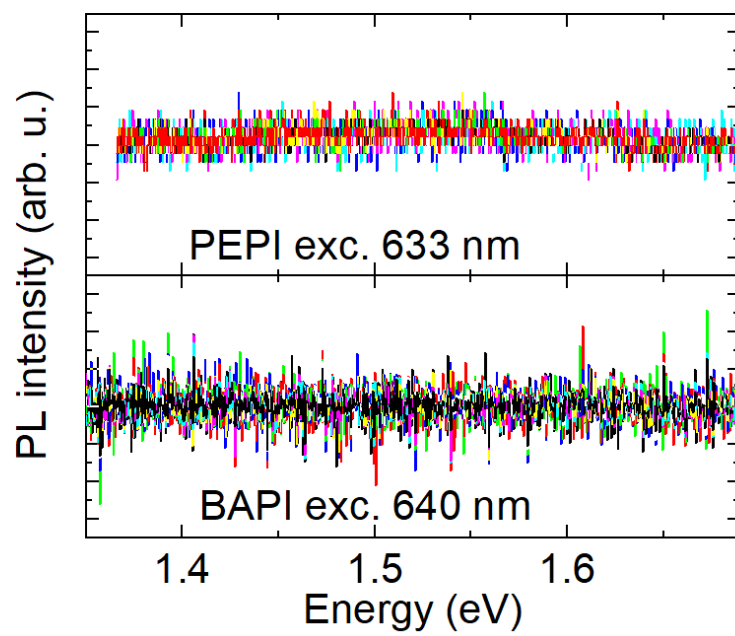


Figure S3: Lack of PL emission in the energy range of IX on bare 2D parts when excited below optical bandgap. Different colors correspond to different spots in bare 2DP flakes.

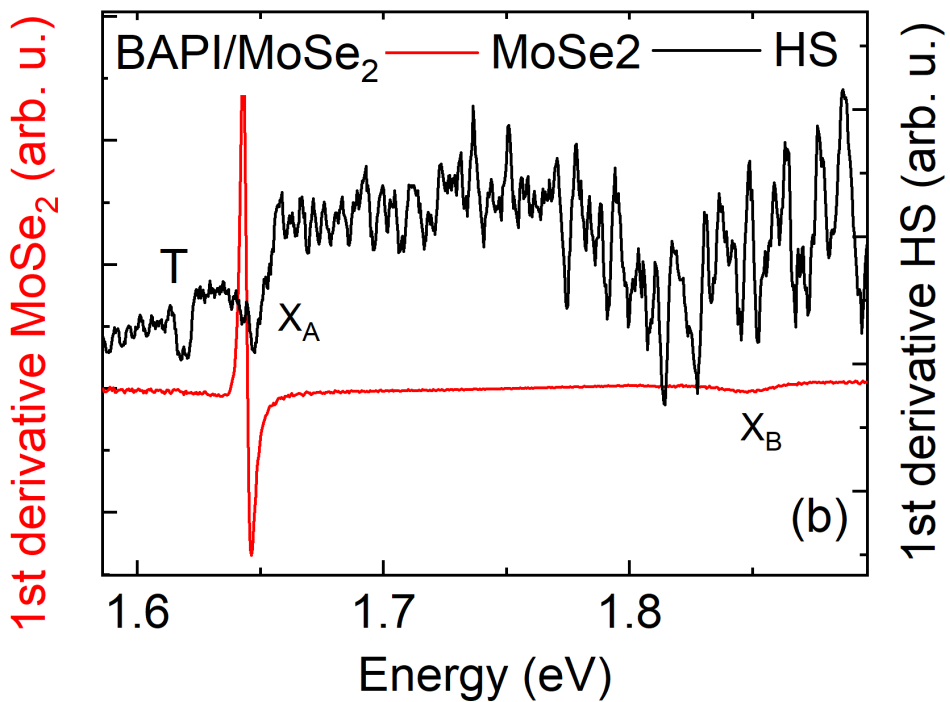
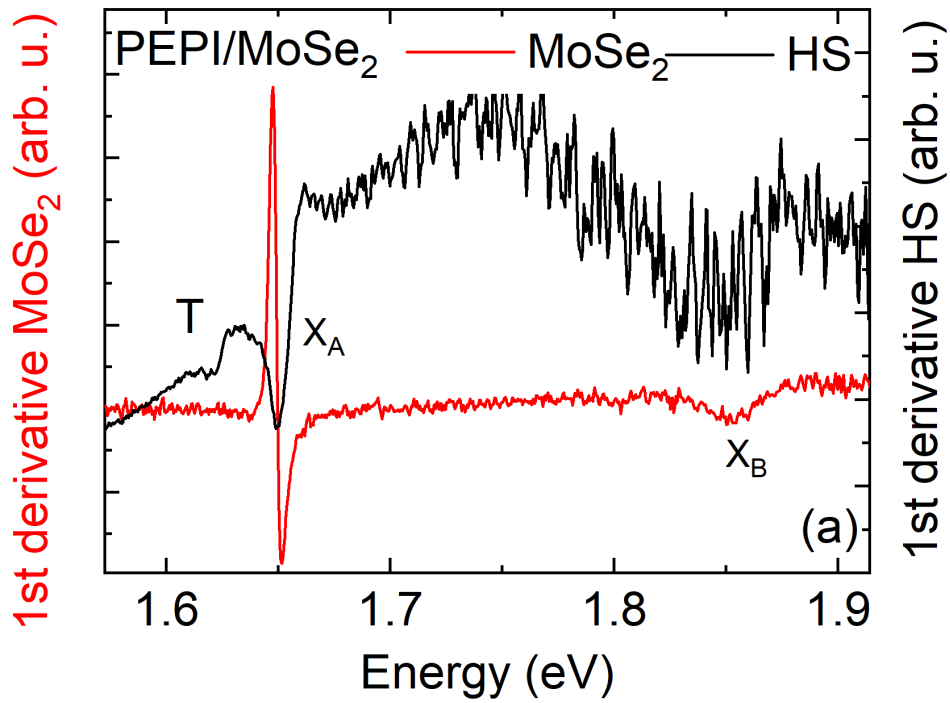


Figure S4: Comparison of 1st derivative of reflectivity spectra on heterostructure (black solid line) and bare  $\text{MoSe}_2$  (red) for PEPI/ $\text{MoSe}_2$  - (a) and BAPI/ $\text{MoSe}_2$  - (b).

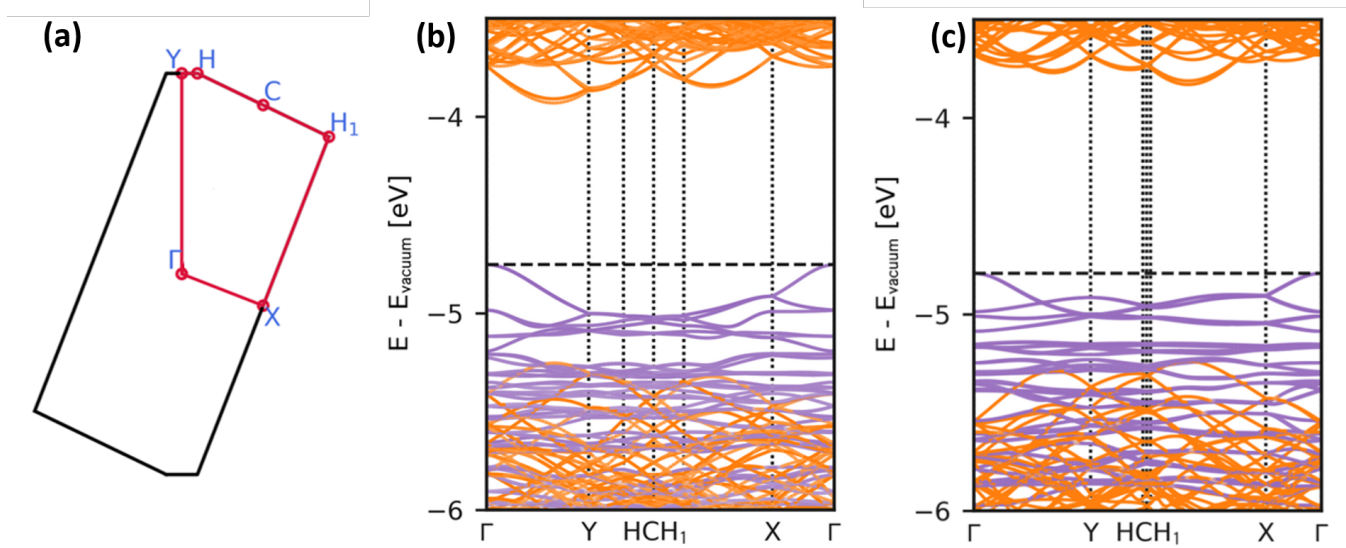


Figure S5: (a) Brillouin zone and  $k$ -path of this low-symmetry model structure. (b) and (c) Mulliken-projected band structure of the PEPI/MoSe<sub>2</sub> and BAPI/MoSe<sub>2</sub> heterostructure showing the majority contributions of each layer.

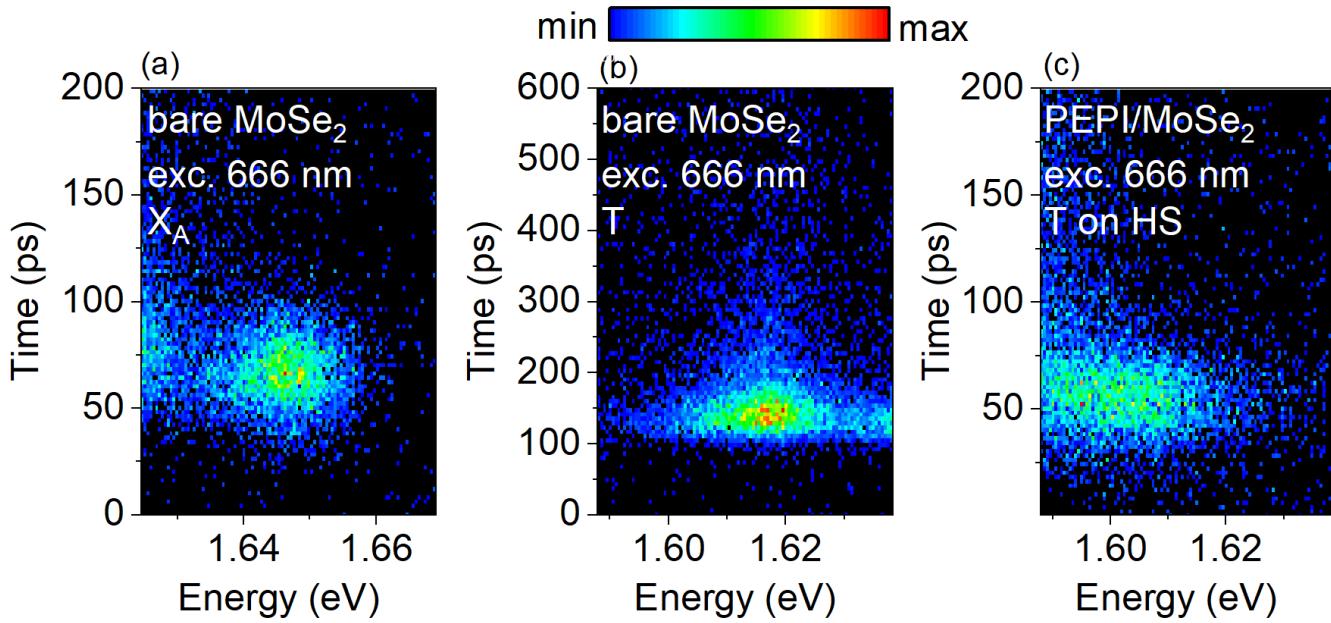


Figure S6: Streak images of MoSe<sub>2</sub> PL decay of  $X_A$  and Trion outside PEPI/MoSe<sub>2</sub> heterostructure (a-b) and Trion decay in heterostructure part.

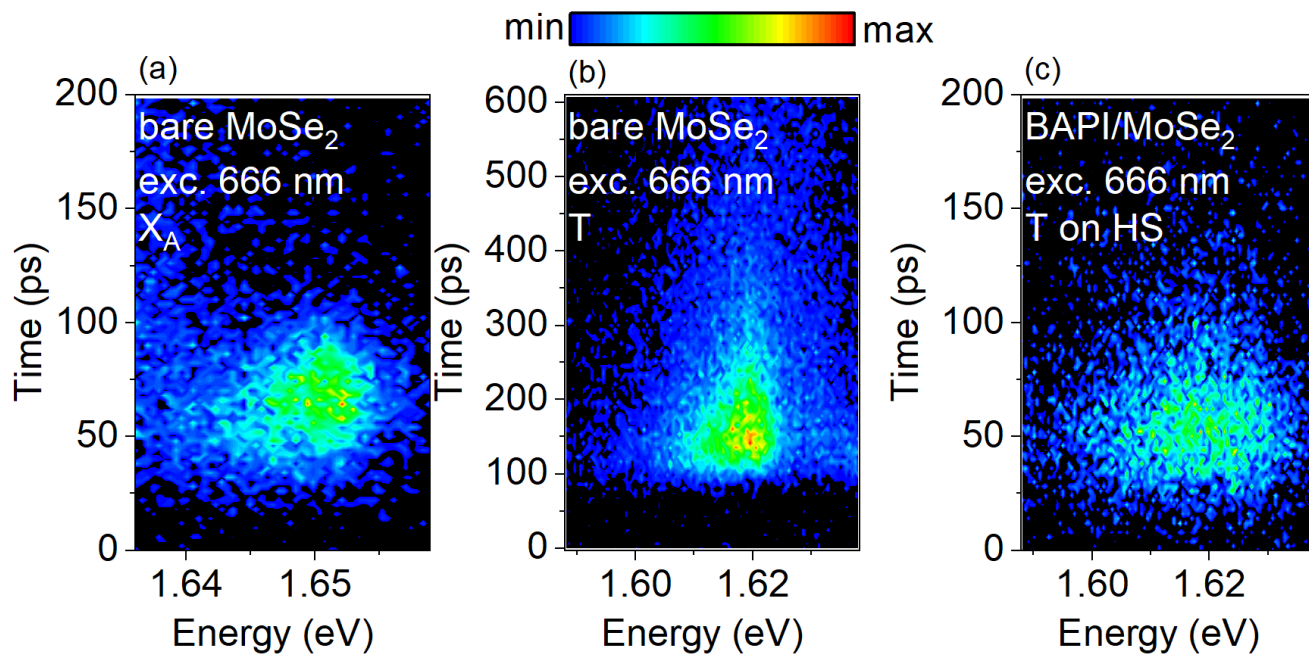


Figure S7: Streak images of MoSe<sub>2</sub> PL decay of  $X_A$  and Trion outside BAPI/MoSe<sub>2</sub> heterostructure (a-b) and Trion decay in heterostructure part.

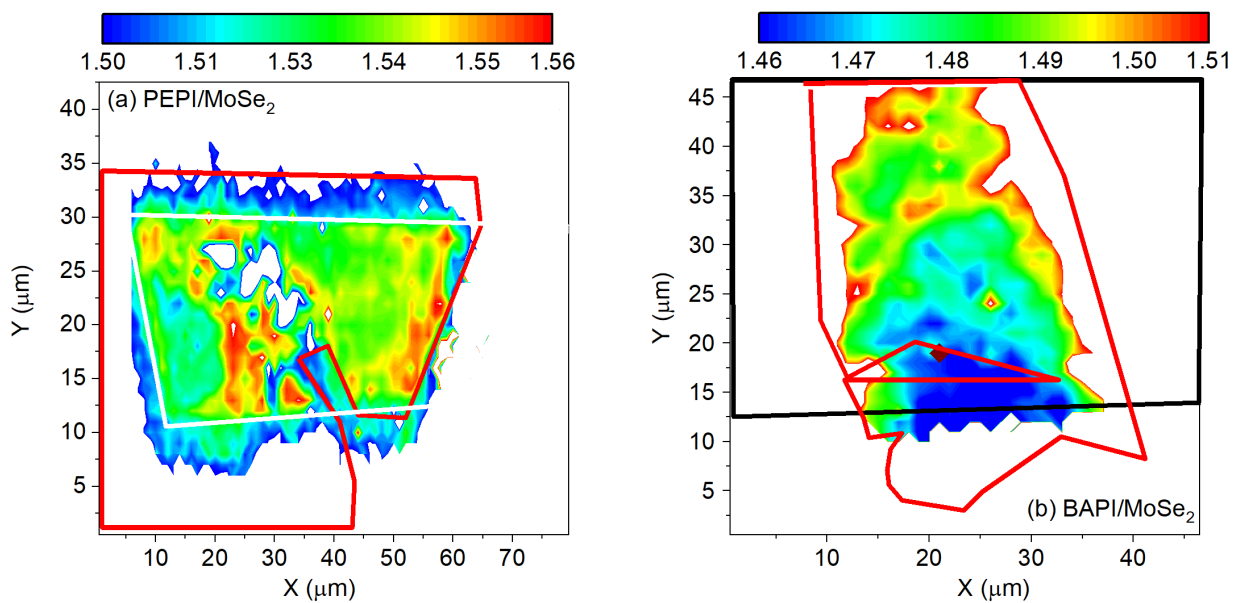


Figure S8: Spatial dependence of the IX PL peak for two investigated heterostructures.